Available on CMS information server

CMS AN -2010/064

The Compact Muon Solenoid Experiment

Analysis Note

The content of this note is intended for CMS internal use and distribution only

09 March 2010 (v2, 09 July 2010)

Effect of muon misalignments on muon p_T resolution and on the search for $Z' \rightarrow \mu^+\mu^-$ in pp collisions at 7 TeV with CMS

Samir Guragain, Marcus Hohlmann

Abstract

This note describes the expected effect of muon misalignments on the search for high-mass resonances decaying to dimuons, in particular $Z' \rightarrow \mu^+\mu^-$ and Drell-Yan events, using fully reconstructed sets of simulated events of proton-proton (pp) collisions at $\sqrt{s}$ = 7 TeV with the CMS experiment at LHC. We study the transverse momentum (p_T) resolution for muons from the Z' decay at different masses and center-of-mass energies using different alignment scenarios and alignment systematics. The simulation results show that the expected p_T resolution for muons in the endcap is about 14.4% (4.8%) with the startup (ideal) alignment scenario using a 1.2 TeV/c^2 Z' sample. The impact of systematic biases in the muon endcap positions and rotations on the p_T resolution is also studied and quantified. The p_T resolution in the endcap for the systematic biases with respect to ideal and startup muon alignment scenarios are presented. With a misalignment of 2 mm in x_{CMS} or y_{CMS} position on ideal alignment scenario of all muon endcap stations, the p_T resolution in the endcap worsens by about 2%. We find a symmetrical effect on resolution with this bias and similar results for biases in x_{CMS} or y_{CMS}, when using the ideal alignment scenario. The startup alignment scenario produces asymmetrical results for biases in x_{CMS} or y_{CMS} and also with positive or negative bias. Using the MC samples, the discovery potential for Z'_{SSM} with different muon misalignments and integrated luminosities is evaluated. We find that a CMS detector better aligned than with the current startup alignment requires significantly less data, i.e. $\sim 250 pb^{-1}$ of integrated luminosity, to discover a Z' signal ($M_{Z'}$ = 1.2 TeV/c^2) with 5σ significance.

1 Introduction

In this note, we study the transverse momentum (p_T) resolution for muons and the dimuon mass resolution for $Z' \rightarrow \mu^+\mu^-$ [1] (spin 1) decays and Drell-Yan events using simulated events of proton-proton (pp) collisions at $\sqrt{s} = 7$ TeV with the CMS experiment. The transverse momentum (p_T) resolution for muons from the Z' decay are studied at different masses and center-of-mass energies using different alignment scenarios. We also discuss the expected effect of systematic muon misalignments on the transverse momentum (p_T) resolution for muons from the Z' decay.

We reconstruct the high-mass dimuon samples with different muon alignment scenarios. We use three standard muon and tracker alignment scenarios, available in the form of global tags [2]. More information about the alignment constants for startup and 50 pb^{-1} alignment scenarios can be found elsewhere [3, 4]. The most relevant items for the muon alignment scenarios and the corresponding global tag, used in this study are briefly mentioned here:

- **Ideal** (MC_31X_V5): corresponding to ideal geometry of the detector
- **Startup** (STARTUP31X_V4): based on CRAFT 2008 and 2009 data analysis for early phase and produced by randomly misaligning chambers with an RMS consistent with cross-checks in the CRAFT 2009

  Uncertainty in CSC chamber positions comes in the following 5 parts:

  1. 0.0092 cm layer x misalignments observed with beam-halo tracks
  2. isotropic photogrammetry uncertainty of 0.03 cm (x, y, z) and 0.00015 rad in ϕ_z
  3. 0.0023 rad ϕ_y misalignment observed with beam-halo tracks
  4. 0.1438 cm z and 0.00057 rad ϕ_x uncertainties between rings from Hardware Straight Line Monitors (from comparison with photogrammetry in 0T data)
  5. 0.05 cm (x, y, z) ME disk misalignments and 0.0001 rad rotation around beamline

  Uncertainty in DT chamber positions comes in the following 2 parts:

  1. Positions within sectors:
     For aligned chambers (wheels -1, 0, +1 except sectors 1 and 7):
     (0.08 cm, 0.1 cm , 0.1 cm) in (x, y, z) and
     (0.0007 rad, 0.0007 rad , 0.0003 rad) in (ϕ_x, ϕ_y, ϕ_z)
     For unaligned chambers
     (0.08 cm, 0.24 cm , 0.42 cm) in (x,y,z) and
     (0.0016 rad, 0.0021 rad , 0.0010 rad) in (ϕ_x, ϕ_y, ϕ_z)
  2. Positions of the sector-groups:
     For aligned chambers: 0.05 cm in x
     For unaligned chambers 0.65 cm in x
  3. Superlayer z uncertainty is 0.054 cm.

- **50 pb^{-1}** (50PBMU31X_V1): Assuming an alignment with tracks using 50 pb^{-1} data and produced by running the Reference-Target algorithm [5] on appropriate MC samples.

  In this scenario, the starting misalignments are (0.2 cm in x, 0.4 cm in y and z, 0.002 rad in ϕ_x, ϕ_y, ϕ_z random Gaussians) in the barrel, and the startup scenarios in the endcap. The first pass of alignment is performed with simulated cosmics. Then, the second and final pass of alignment is performed with simulated collision muons by allowing the following parameters to float:

1. DT stations 1-3: x, y, ϕ_x, ϕ_y, ϕ_z (inherit z from cosmics alignment)
2. DT station 4: x, ϕ_y, ϕ_z (others are still misaligned)
3. CSCs: x, ϕ_y, ϕ_z (inherit z and ϕ_x from hardware)

In the final result [6], this procedure yields the following uncertainties:

1. 0.04894 cm in x: all aligned chambers (everything but ME1/3 and one fit failure: ME-1/4, 8)
2. 0.09552 cm in y: wheels -1, 0, 1, stations 1-3 (only showing the ones with a reliable z alignment from cosmic rays)
3. 0.1826 cm in z: same as in y
4. 0.000366 rad in ϕ_x: DT stations 1-3
5. 0.000266 rad in ϕ_y: all aligned chambers
6. 0.0005976 rad in ϕ_z: all aligned chambers

The remaining parameters are similar to the startup scenario.

Tracker misalignment scenarios [7] in startup and 50 pb^{-1} alignments are the same and based on CRAFT 2008. The scenario describing the misalignment of the tracker at the CMS startup (also known as "TrackerCRAFTScenario" with the tag TrackerCRAFTScenario310_mc) consists of segments of already existing scenarios for each of the tracker subdetector based on the distributions of residuals observed after the alignment of the Tracker with the data from CRAFT 2008 (about 4 million cosmic tracks).

Misalignments of the tracker and of the muon system in the early stages of collision data taking have been taken into account by using the so-called "startup" and "50 pb^{-1}" misalignment scenarios, which give estimates of the alignment achieved at startup and with an integrated luminosity of 50 pb^{-1}, respectively. In order to study the effect of systematic misalignment in the muon endcap system on the muon p_T resolution, we reconstruct the 1.2 TeV/c^2 and 2.0 TeV/c^2 Z' samples with the above mentioned misalignment scenarios and re-run the standard Zprime2muAnalysis [8] package, in particular the Zprime2muResolution code over the resulting simulated data sets. These muon misalignment scenarios are simulated separately with respect to ideal and startup scenarios. Since the startup alignment scenario is already biased, we use ideal alignment scenario as well. To simulate a misaligned muon endcap system, individual muon endcap yoke disks (stations) and entire endcaps are misaligned in position (x_{CMS}, y_{CMS}, z_{CMS}) up to $\pm$ 2 mm or rotated around the beam line, i.e. rotation angle $\phi_{z_{CMS}}$ up to $\pm$ 0.5 mrad with steps of 0.1 mm or 0.1 mrad, respectively.

The observability of the $Z' \rightarrow \mu^+\mu^-$ channel with the CMS experiment has been studied previously [9–11] at $\sqrt{s}$ = 14 TeV and also at $\sqrt{s}$ = 6 and 10 TeV [12]. In this study, we update the potential of the CMS experiment to discover an additional heavy neutral gauge boson Z' in proton-proton (pp) collisions at $\sqrt{s}$ = 7 TeV using Monte Carlo samples for this center-of mass energy. Finally, we present our studies of how muon misalignments could effect the signal significance.

2 Monte Carlo samples

All signal and background samples used in this study are generated with PYTHIA [13] version 6.4 (with photon emission off incoming or outgoing quarks and leptons switched on) and the CTEQ6L set of parton distribution functions (PDF) [14] from LHAPDF [15] version 5.6.0. From a large variety of new heavy resonances described in [1, 16] we choose the Z'_{SSM} within the Sequential Standard Model (SSM) [17], which has the same couplings as the Standard Model Z^0 and is often used as a benchmark by experimentalists. It is available in the PYTHIA generator [13]. The detector response is simulated with the GEANT4-based simulation sub-package of CMSSW [18], version 3_1_0. The digitization (simulation of the electronics response), the emulation of the Level- 1 and High-Level (HLT) Triggers, and the offline reconstruction are performed with the full CMS reconstruction package CMSSW [18], version 3_1_0.

We make the usual assumption that the resonances decay only to three ordinary families of quarks and leptons and that no exotic decay channels are open. The cross sections for Z'_{SSM} is shown in Table 1 are at leading order (LO), as predicted by PYTHIA. We scale them by a constant K factor of 1.35 in order to take into account the next-to-next-to-leading order (NNLO) QCD corrections. The full-interference $Z'/Z^0/\gamma^*$ samples used in this study are generated in broad mass intervals around the mass peak (above 400 GeV/c^2 for $M_{Z'}$ = 1 TeV/c^2, above 600 GeV/c^2 for $M_{Z'}$ = 1.2 TeV/c^2 and 1.3 TeV/c^2, and above 1 TeV/c^2 for $M_{Z'}$ = 2 TeV/c^2).

Table 1: The product of the leading-order production cross section times branching ratio for Z'_{SSM} with masses $M_{Z'}$ of 1.0, 1.2, 1.3 and 2 TeV/c^2 for 7 TeV center-of-mass energy, as predicted by PYTHIA.

$M_{Z'_{SSM}}$ [TeV/c^2]	1.0	1.2	1.3	2.0
$\sigma^{LO}\times$ BR [fb] (PYTHIA)	137	40	29	2

The dominant (and irreducible) source of background to new high-mass dimuon resonances is Drell-Yan production of muon pairs, $pp \to \gamma^*/Z^0 \to \mu^+\mu^-$. Drell-Yan samples with two different cut-off values on the dimuon invariant mass are generated: $M_{\mu^+\mu^-} \geq 0.2, 0.5$ TeV/c^2. The total production cross section times branching ratio in these two mass intervals are listed in Table 2.

Each of these samples including Z'_{SSM} signal samples has 50,000 events unless otherwise mentioned. These samples are reconstructed with ideal, startup, and 50 pb^{-1} alignments. All of these samples are hosted by T3_US_FIT and are available in the Database Bookkeeping System (DBS) at DBS instances of cms_dbs_ph_analysis_02.

Table 2: The product of the leading-order production cross section times branching ratio for Drell-Yan events with different cut-off values on the dimuon mass for 7 TeV center-of-mass energy, as predicted by PYTHIA.

$M_{\mu^+\mu^-}$ [TeV/c^2]	≥ 0.2	≥ 0.5
$\sigma^{LO}\times$ BR [fb] (PYTHIA)	1052	26

3 Event selection

In order to select efficiently a pure sample of high-mass dimuon candidates, we require that:

- The event pass the logical OR of single-muon and dimuon non-isolated trigger paths.
- It contain at least one pair of oppositely-charged muons reconstructed offline.
- The transverse momentum p_{T} of each muon track in a pair be larger than 20 GeV/c.
- Both muons be isolated in the tracker in such a way that the sum of the p_{T} of all tracks around each muon in a cone of $\Delta R = \sqrt{(\Delta\phi)^2 + (\Delta\eta)^2} < 0.3$ is required to be less than 10 GeV/c.

4 Results for muon p_T and dimuon mass resolutions with misalignments

The precision of reconstructed dimuon mass and consequently the statistical significance of a possible resonance peak is affected by imperfect alignment of the tracker and the muon spectrometer. Small curvatures of high-momentum tracks would be poorly constrained if the alignment of sensor and chamber positions is uncertain; a situation we expect to improve with a good amount of data.

To describe the expected misalignments and their improvement with time and integrated luminosity, several misalignment scenarios were developed in the CMS reconstruction framework in previous studies [9, 19, 20]. These misalignment scenarios are updated here to simulate the detector alignment expected to be achieved at startup and with 50 pb^{-1} of integrated luminosity. These updated scenarios take into account alignment expertise accumulated since the Physics TDR and, in particular with the results obtained during the Magnet Test and Cosmic Challenge (MTCC), and the Cosmic Run At Four Tesla (CRAFT) in 2008 and 2009. The results and the hardware constants derived from the muon alignment system in CRAFT 2008 are described in [21]. The uncertainties in the positions of muon chambers resulting from these alignment scenarios are then used in the reconstruction of high-p_T muons from Z' decays, with the corresponding tracker misalignment, to measure the transverse momentum resolution and the dimuon mass resolution.

The relative transverse momentum (p_T) resolution is obtained by a Gaussian fit to the distribution of the quantity

$$\left(\frac{q/p_T^{rec} - q/p_T^{gen}}{q/p_T^{gen}}\right), \tag{1}$$

where q is the muon charge, and p_T^{gen} and p_T^{rec} are the generated and reconstructed transverse momenta, respectively.

The dimuon mass resolution is obtained by a Gaussian fit to the distribution of the quantity

$$\left(\frac{M_{\mu^+\mu^-}^{rec} - M_{\mu^+\mu^-}^{gen}}{M_{\mu^+\mu^-}^{gen}}\right), \tag{2}$$

where $M_{\mu^+\mu^-}^{gen}$ and $M_{\mu^+\mu^-}^{rec}$ are the generated and reconstructed dimuon masses, respectively.

Before calculating the invariant mass of an opposite-sign muon pair, $M_{\mu^+\mu^-}$, a search for photon candidates in a cone with a radius of $\Delta R < 0.1$ around the trajectory of each muon is performed, and the 4-momentum of the photon candidate with the smallest ΔR in the cone is added to the 4-momentum of the muon. This procedure improves the invariant mass resolution by recovering some of the energy lost by the muon via final state radiation and radiative processes in the detector.

4.1 Z' signal

The dimuon mass resolution and transverse momentum resolution for muons from Z' decay with several misalignment scenarios are presented in this section. One of the events from the simulated Z' with mass 1.2 TeV/c^2 decaying to two high p_T muons is shown in Figure 1.

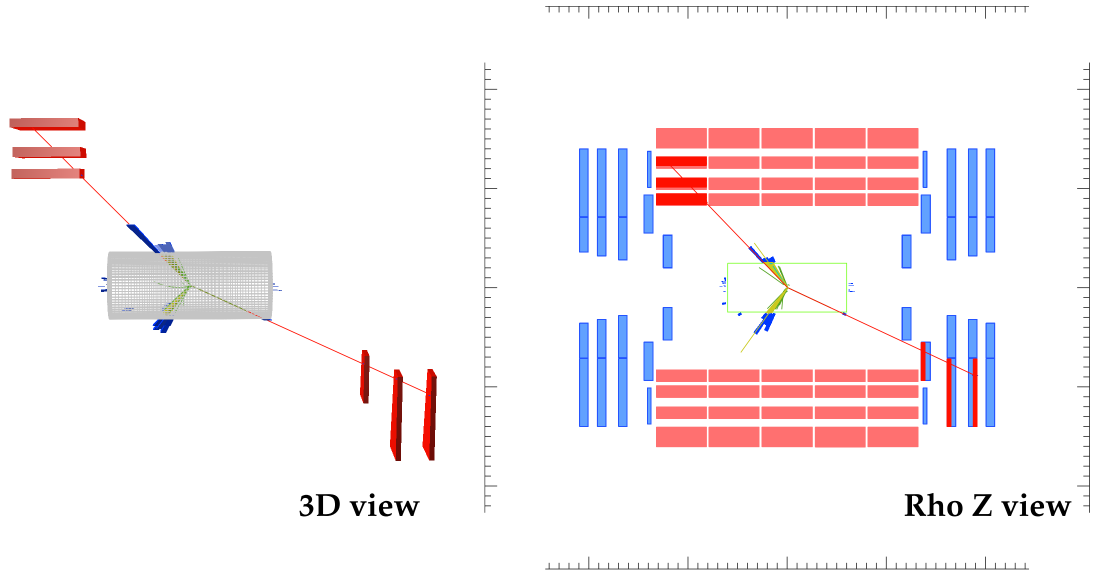

Figure 1: A simulated Z' event with $M^{gen}_{\mu^+\mu^-}$ = 1105 GeV/c^2 in CMS, showing two high p_T (361.5 GeV/c and 354.5 GeV/c) muons (red lines) in two views. The event is reconstructed with startup alignment and the globally reconstructed dimuon mass is $M^{rec}_{\mu^+\mu^-}$ = 1078 GeV/c^2.

The invariant mass resolution depends on the alignments of the silicon tracker and of the muon system. The dimuon mass resolution for 1.2 TeV/c^2 Z'_{SSM} resonance are shown in figure 2 illustrating how the expected misalignment smears the distribution of the mass resolution. Current estimates of the alignment expected to be achieved with 50 pb^{-1} of integrated luminosity predict a mass resolution of 6-7% at $M_{\mu^+\mu^-}$ = 1 TeV/c^2. We calculate the dimuon mass resolutions for a number of cases, with three alignment scenarios for three Z' signal mass points at 10 TeV and 7 TeV center-of-mass energy. They are tabulated in Table 3 as obtained from three muon reconstruction algorithms; Global reconstruction (GR), Tracker only (TK) and tracker-plus-first-muon station (FS) [22].

We have also studied the transverse momentum resolutions for muons from the Z' decay for various combinations of alignments, center-of-mass energies, and Z' masses. The p_T resolutions are studied separately in the endcap and barrel regions. We are mostly focusing on the endcap. The p_T resolutions for the endcap muons are shown in Figure 3, where the effect of misalignments is clearly seen.

Table 3 summarizes also our studies for muon p_T resolutions in the endcap at 7 TeV and 10 TeV center-of-mass energies with three alignment scenarios (ideal, startup, and the 50 pb^{-1}) for three Z' signal samples ($M_{Z'}$ = 1.0, 1.2, 1.3 TeV/c^2). The last three columns show the momentum resolutions as obtained from three muon reconstruction algorithms; Global reconstruction

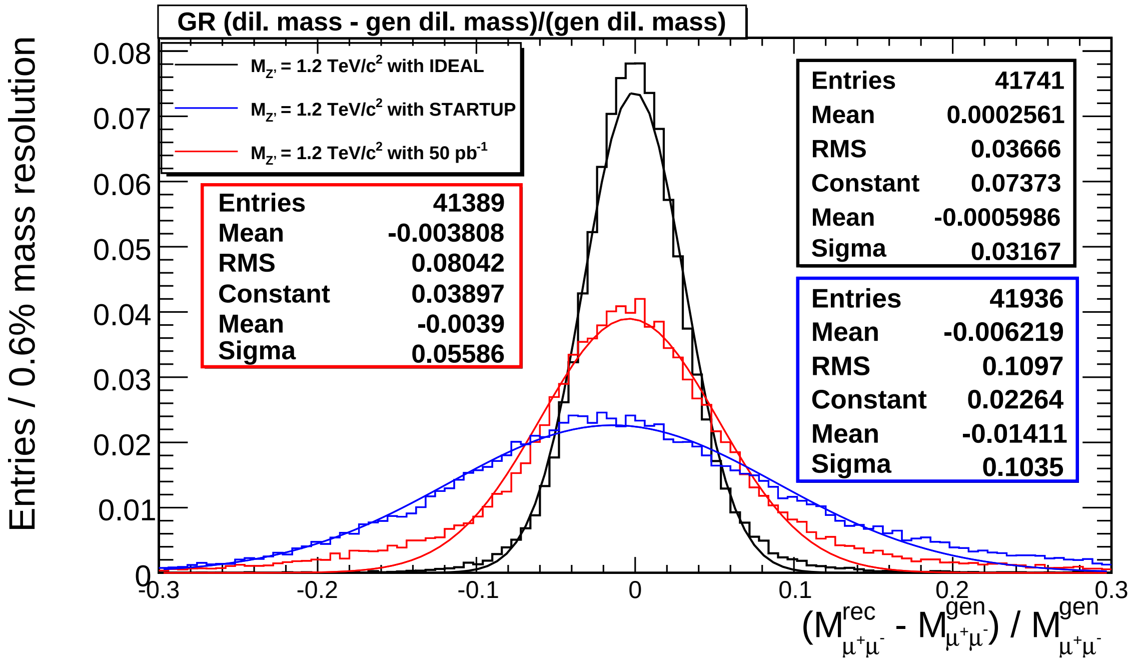

Figure 2: Normalized invariant mass resolution for 1.2 TeV/c^2 Z'_{SSM}. The events shown here are reconstructed with three alignment scenarios: ideal (black), startup (blue) and 50 pb^{-1} (red) indicating the considerable effect of muon misalignment.

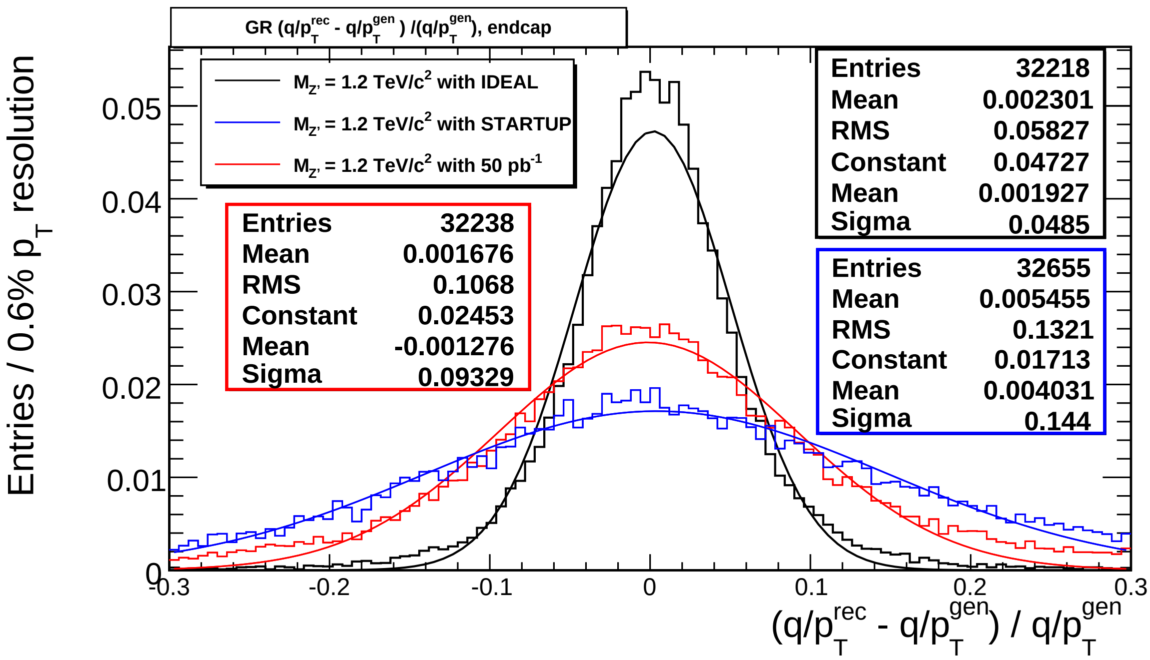

Figure 3: Normalized relative p_T resolution for endcap muons from 1.2 TeV/c^2 Z'_{SSM} simulated with three different alignment scenarios: ideal (black), startup (blue) and 50 pb^{-1} (red).

Table 3: Summary of Z' mass and muon endcap p_T resolution studies for different alignment scenarios, muon reconstruction algorithms (global reconstruction "GR", Tracker only "TK", and tracker plus the first muon station "FS") and center-of-mass energies.

Z′ Mass	Alignment	CM energy	Dimuon Mass Resolution (%)			Muon Endcap p_T Resolution (%)		
(TeV/c²)	Scenario	(TeV)	GR	TK	FS	GR	TK	FS
1.0	IDEAL	10	3.0	3.5	2.9	4.6	5.1	4.5
		7	2.6	3.1	2.5	3.9	4.4	3.8
	50 pb^{-1}	10	6.6	11.1	6.0	10.6	16	9.9
		7	6.2	9.4	5.2	9.8	13.6	8.9
	STARTUP	10	10.2	11.1	8.5	13.9	16	10.9
		7	8.9	9.4	7.4	12.9	13.4	9.7
1.2	IDEAL	10	3.0	3.5	2.9	4.6	5.1	4.5
		7	3.2	3.9	3.1	4.8	5.1	4.7
	50 pb^{-1}	10	6.7	11.1	6.0	10.6	16	9.9
		7	5.6	11.2	6.1	9.3	14.9	9.4
	STARTUP	10	10.2	11.1	8.5	13.9	16	10.9
		7	10.3	11.4	8.1	14.4	15.9	9.9
1.3	IDEAL	10	3.4	4.4	3.3	5.3	6.3	5.2
		7	3.2	4.1	3.1	4.4	4.9	4.4
	50 pb^{-1}	10	6.7	13.3	6.3	10.7	18.9	10.6
		7	6.0	11.3	5.7	8.4	16.1	9.4
	STARTUP	10	11.8	13.3	10.3	15.2	18.9	12.0
		7	10.5	11.3	9.6	14.2	16.2	10.4

(GR), Tracker only (TK) and tracker-plus-the-first-muon station (FS). From Table 3 we conclude that

- Resolutions improve significantly from the startup alignment to the 50 pb^{-1} alignment
- For a given alignment, the resolutions basically do not depend on the center-of-mass energy
- Inclusion of the first muon station in the track fit improves the resolution drastically, which illustrates the importance of muon tracking for high p_T muons

4.2 High-mass Drell-Yan background

The globally reconstructed (GR) invariant mass spectra for Drell-Yan events with $M^{gen}_{\mu^+\mu^-} > 500\,GeV/c^2$ are shown in Figure 4. The global muon reconstruction uses information for the muon system and also silicon tracker hits. The reconstruction is performed with three different alignment scenarios: ideal, startup, and 50 pb^{-1}.

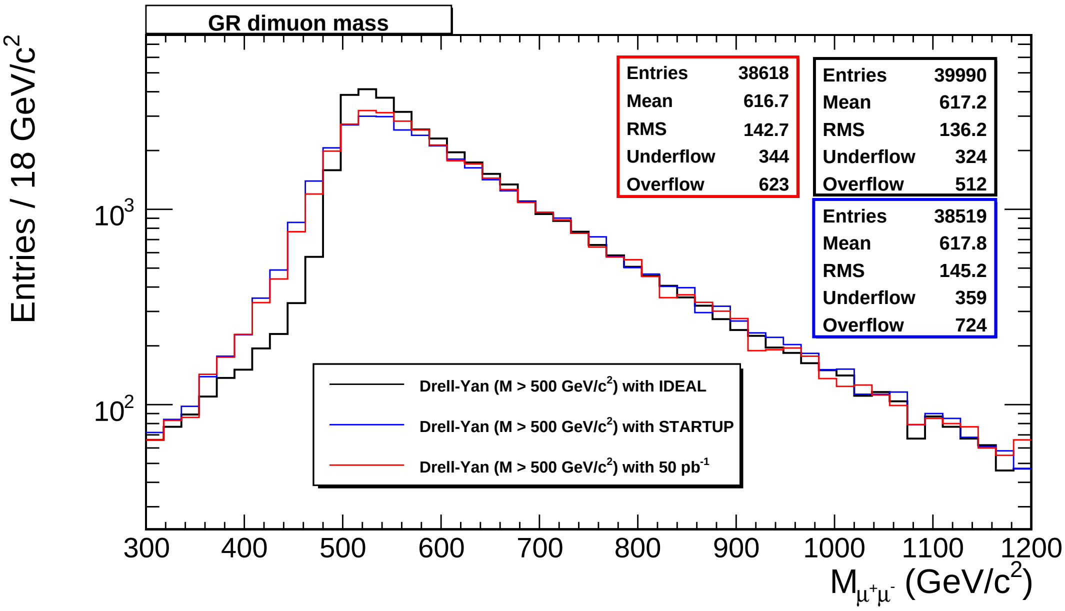

Figure 4: The globally reconstructed (GR) invariant mass spectra for the Drell-Yan events with invariant mass $M^{gen}_{\mu^+\mu^-} > 500$ GeV$/c^2$. The alignment scenarios are ideal (black), startup (blue), and 50 pb^{-1} (red). These plots are normalized to the same number of events.

The p_T resolutions are studied separately in the endcap and barrel regions. We mostly focus on the endcap here. The global muon p_T resolutions in the Barrel and Endcap for Drell-Yan events with $M^{gen}_{\mu^+\mu^-} > 500$ GeV$/c^2$ with three different alignments are shown in figure 5. The p_T resolutions in the Barrel and Endcap for the startup scenario are 6.6% and 11.5%, respectively. In the endcap, the resolutions for each alignment are worse than those in the barrel, as expected.

The mass resolution spectra for Drell-Yan with $M^{gen}_{\mu^+\mu^-} > 500$ GeV$/c^2$ are shown in Figure 6. The spectra show considerable impact of muon and tracker misalignments for the different alignment scenarios. The invariant mass resolutions for Drell-Yan events with $M^{gen}_{\mu^+\mu^-} > 500$ GeV$/c^2$ for ideal, startup, and 50 pb^{-1} are found to be 2.3%, 7.3%, and 5.3%, respectively.

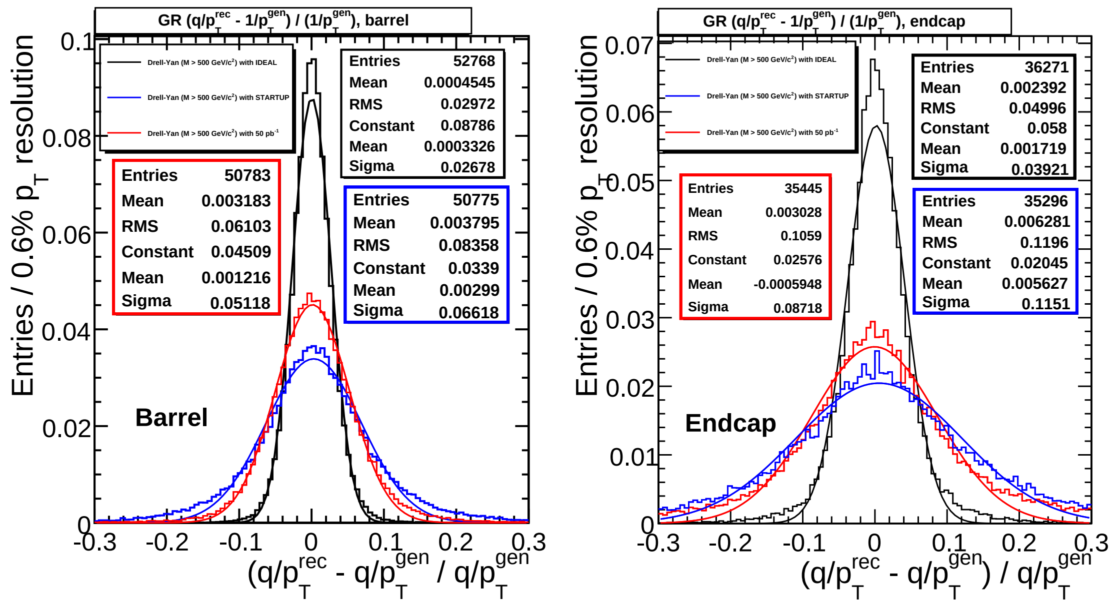

Figure 5: Normalized p_T resolution spectra for muons in Barrel only (left) and Endcap only (right) for Drell-Yan events with $M^{gen}_{\mu^+\mu^-} > 500$ GeV$/c^2$ at $\sqrt{s}$ = 7 TeV. The events shown here are for ideal (black), startup (blue), and 50 pb^{-1} (red) alignment scenarios. The p_T resolutions for muons in the endcap are 3.9%, 11.5%, and 8.7% for ideal, startup, and 50 pb^{-1} alignment scenarios, respectively.

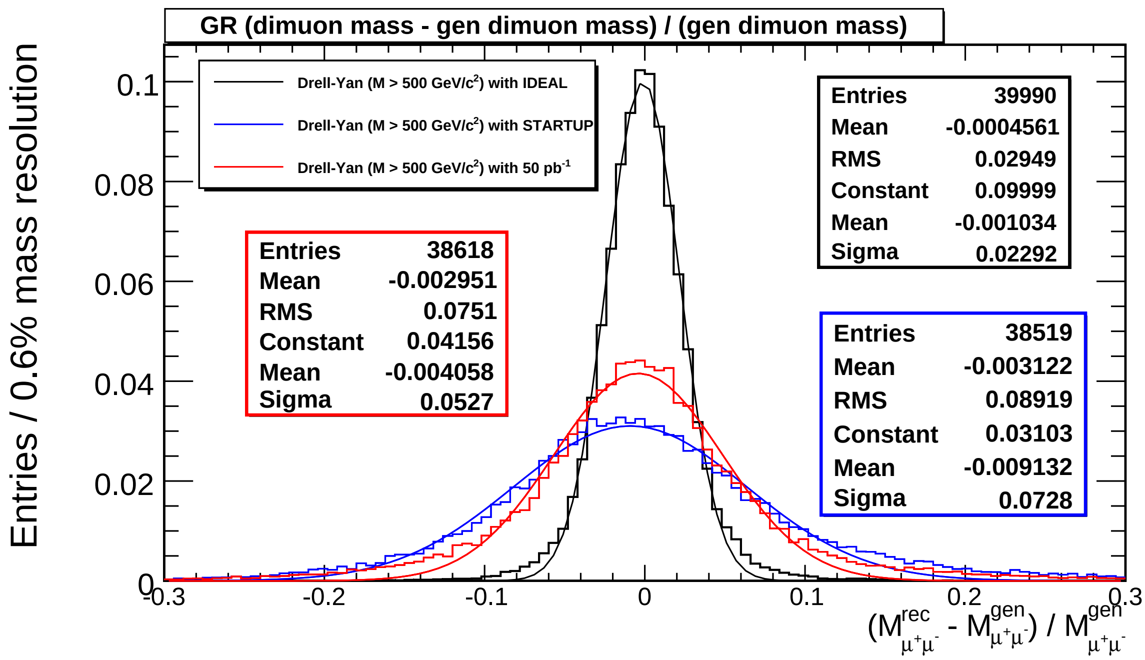

Figure 6: The invariant mass resolution spectra for Drell-Yan events with $M^{gen}_{\mu^+\mu^-} > 500$ GeV$/c^2$ at $\sqrt{s}$ = 7 TeV. The events shown here are reconstructed with three alignment scenarios: ideal (black), startup (blue) and 50 pb^{-1} (red) indicating the considerable effect of muon misalignment in the different scenarios.

5 Muon Endcap alignment systematics and p_T resolution

We have studied the impact of anticipated muon endcap alignment systematics, i.e. how systematic biases in the muon endcap positions will affect the muon p_T resolutions. For this study, only the muon endcap is misaligned with respect to the existing ideal or startup muon geometry. Individual muon endcap yoke disks (stations) and also entire endcaps are misaligned in position (x_{CMS}, y_{CMS}, z_{CMS}) up to ± 2 mm or rotated in $\phi_{z_{CMS}}$ i.e. around the beam line, up to ± 0.5 mrad with steps of 0.1 mm and 0.1 mrad, respectively. The selection of these numbers is motivated by the current startup muon endcap alignment uncertainties, which are 0.5 -1.0 mm in position (Δx_{CMS}, Δy_{CMS}, Δz_{CMS}) and 0.1 mrad in $\Delta\phi_{z_{CMS}}$. These numbers are also motivated by the CRAFT 2008 study [21]. A recently discovered bug in the track-based alignment procedure related to the inclusion of RPC hits in the track fitting indicated a systematic alignment shifts up to 1.5 mm [23], i.e. of similar magnitude.

The method for this study is as follows:

1. A standard CMSSW-readable muon geometry in an SQLite file is converted into a human-readable XML file using a tool described in [24]. The XML file is modified according to our intended misalignments and converted back to an SQLite file. Thus, a modified muon geometry with each intended misalignment is generated and saved in the form of an SQLite database file.

2. A Z' signal sample ($M_{Z'_{SSM}}$ = 1.2 TeV/c^2 or 2.0 TeV/c^2) is fully reconstructed with a customized global tag with modified SQLite file corresponding to the ideal or startup alignment.

3. The analysis code is re-run over the resulting biased MC data set for each case repeatedly. We obtain the results for different reconstructions: Global reconstruction (GR), Tracker-only (TK) and Tracker plus the First Muon Station (FS). Tracker-only (TK) is driven by measurements in the silicon tracker only. Global muon reconstruction (GR) is based on a combined fit to selected hits in the muon system and the silicon tracker. Another approach of refitting the global-muon track ignoring hits in all muon stations except the innermost one containing hits is called the "tracker plus the first muon station" (FS) fit.

First, we verify our procedure by comparing the results with bias in the endcap and without the bias. In order to do so, we have to get identical results in the barrel and tracker-only reconstruction results, where we are not imposing any bias. We plot the width of relative muon p_T resolutions as a function of pseudorapidity (η) in Figure 7. We see exactly the expected results in Figure 7, where the top plot is without bias (ideal alignment) and the bottom plot is with 2 mm systematic bias to all Muon Endcap stations in x_{CMS}. The central regions are identical in both plots but in the endcap ($|\eta| > 1$) the resolutions have become worse due to the bias except in the tracker-only reconstruction, as expected. These facts confirm that the reconstruction is performing as intended.

Next, we discuss p_T resolutions as a function of p_T. Again, we compare the results with the bias and without it. Figure 8 shows the comparison of the Gaussian widths of q/p_T relative resolution for muons in each p_T bin with and without bias for ideal alignment. It is clearly seen that the bias of 2 mm deteriorates the muon p_T resolutions. This effect becomes significant for $p_T > 200$ GeV/c. Since we are concerned with different alignment scenarios, the most relevant scenario to study the effect of misalignment is the startup alignment. The corresponding plot for the muon p_T resolution vs. p_T using the decay of a 2 TeV/c^2 Z' but reconstructed with startup alignment is shown in Figure 9. We get a resolution of 10-20% for $p_T > 200$ GeV/c with startup alignment, whereas 4-6% is found with ideal alignment for the same p_T range.

Table 4: Gaussian width (σ) of relative p_T resolution in (%) in the Endcap for biases on all eight Muon Endcap station positions for ideal and startup alignment geometries.

Bias Δx_{CMS} [mm]	0	2.0	-2.0	1.5	-1.5	1.0	-1.0	0.5	-0.5
Ideal	4.8	6.5	6.6	6.2	6.2	5.7	5.7	5.1	5.1
Startup	14.9	18.4	15.8	17.9	14.9	17	14.4	16	14.3

Table 5: Gaussian width (σ) of relative p_T resolution (%) in Endcap for biases on all eight Muon Endcap station orientations for ideal and startup alignment geometries.

Bias $\Delta\phi_{z_{\text{CMS}}}$ [mrad]	0	0.5	-0.5	0.4	-0.4	0.3	-0.3	0.2	-0.2	0.1	-0.1
Ideal	4.8	7.4	7.4	7	7	6.3	6.4	5.9	5.6	5.1	5.1
Startup	14.9	20.5	17.6	18.9	16.4	17.4	15.5	16.2	15	15.4	14.8

More specifically, we quantify the effect of bias in the muon endcap alignment on the p_T resolution for muons in the endcap. We bias the position of one endcap station (eg. ME+1 only) or all endcap stations in x_{CMS} with respect to ideal (or startup). Using the 2 TeV/c^2 Z' sample we analyze the Gaussian width of relative resolution for endcap muons repeatedly with biases of different sizes (0.5 - 2 mm). Also, we bias the position of entire endcap stations and repeat the analysis procedure. We plot the p_T resolution for muons in the endcap as a function of bias in x_{CMS} and $\phi_{z_{CMS}}$ in figure 10 where we present the effect of biases on the position of entire endcap stations and individual station ME+1, ME-1, ME+2, and ME-2. The largest effect is seen when all muon endcaps are biased together as expected. With a similar bias to either ME+1 or ME-1, the effect is identical, which is also true for ME2. The effect becomes less significant as the biased station is farther from the interaction point. Table 4 summarizes the p_T resolution in % for each bias in the position x_{CMS} of the entire endcap with respect to ideal and startup alignment scenarios. As we increase the bias, it deteriorates the muon p_T resolution by 2% for 2 mm systematic bias in x_{CMS} to all muon endcap stations for an ideal alignment. We find similar results with the bias in the position y_{CMS} as with the bias in position x_{CMS} for an ideal alignment. We find insignificant change on the p_T resolution for muons when we bias the position of the entire endcaps in z_{CMS}. Similarly, Table 5 summarizes the p_T resolution in % for each bias in the rotation $\phi_{z_{CMS}}$ of the entire endcap with respect to ideal and startup alignment scenarios.

With respect to ideal alignment, we find symmetrical results but asymmetric results with respect to the startup for the same positive and negative bias as shown in figure 11. In figure 11, we summarize our systematic study of biases on muon endcap disk positions x_{CMS}, y_{CMS}, and z_{CMS} to all endcap stations or individual station ME+1, ME-1, ME+2, and ME-2 with respect to startup alignment. When we bias the position of all stations by 2 mm, the muon p_T resolution in the endcap worsens by 3%. In the case of startup alignment, we bias the position of disks in x_{CMS} and y_{CMS} and quantify their effect on the muon p_T resolution. We find asymmetrical results for positive bias and negative bias and also for the same bias in x_{CMS} and y_{CMS}.

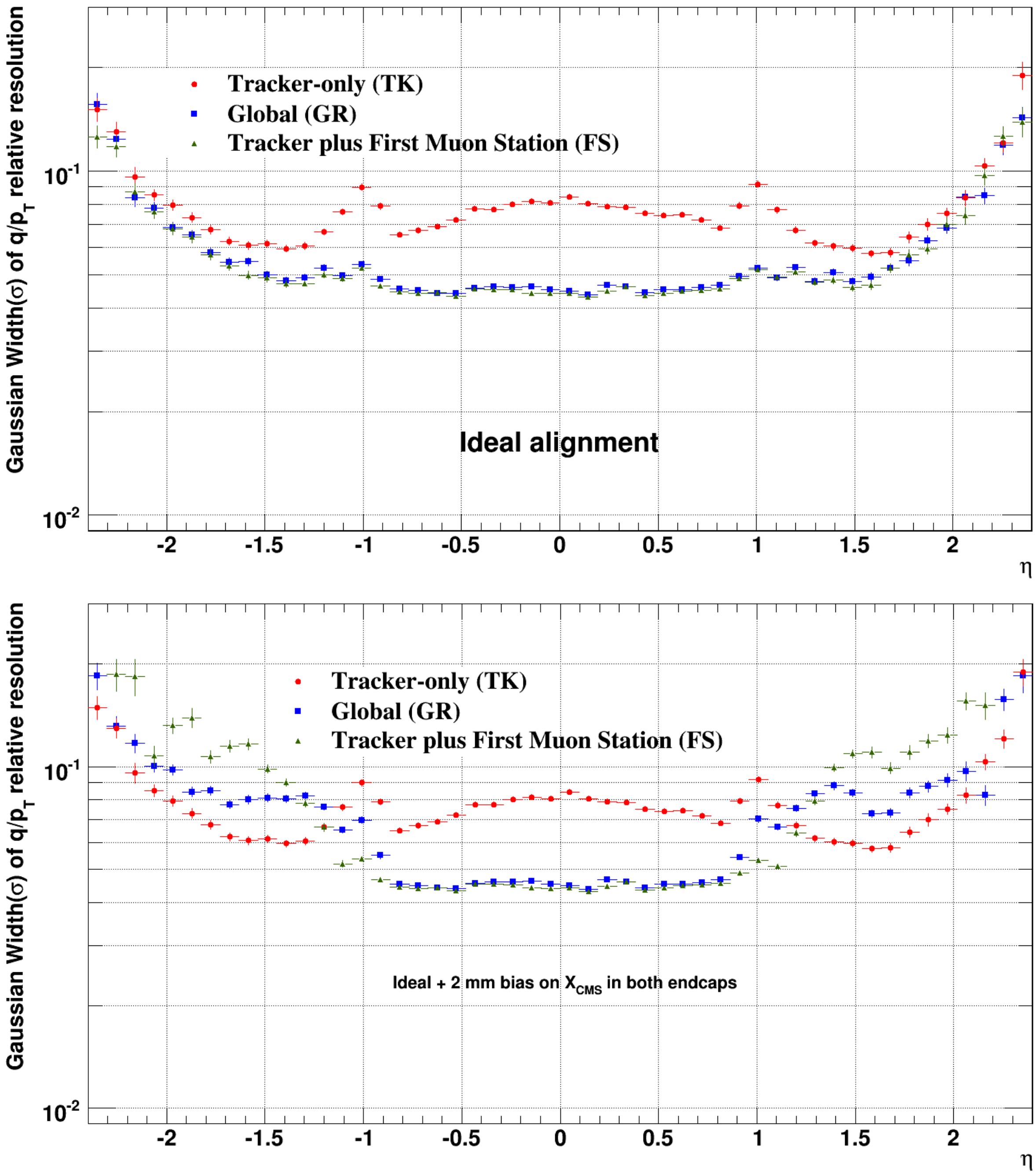

Figure 7: Relative muon p_T resolution vs. η for barrel and endcap muons based on Gaussian widths of $(q/p_T(\text{rec.})\ \text{-}\ q/p_T(\text{gen.}))/q/p_T(\text{gen.})$ distributions for each p_T bin using the MC sample for $M_{Z'} = 2$ TeV$/c^2$ and three muon reconstructions for ideal alignment scenario (top) and with 2 mm systematic bias in x_{CMS} to all Muon Endcap stations (bottom)

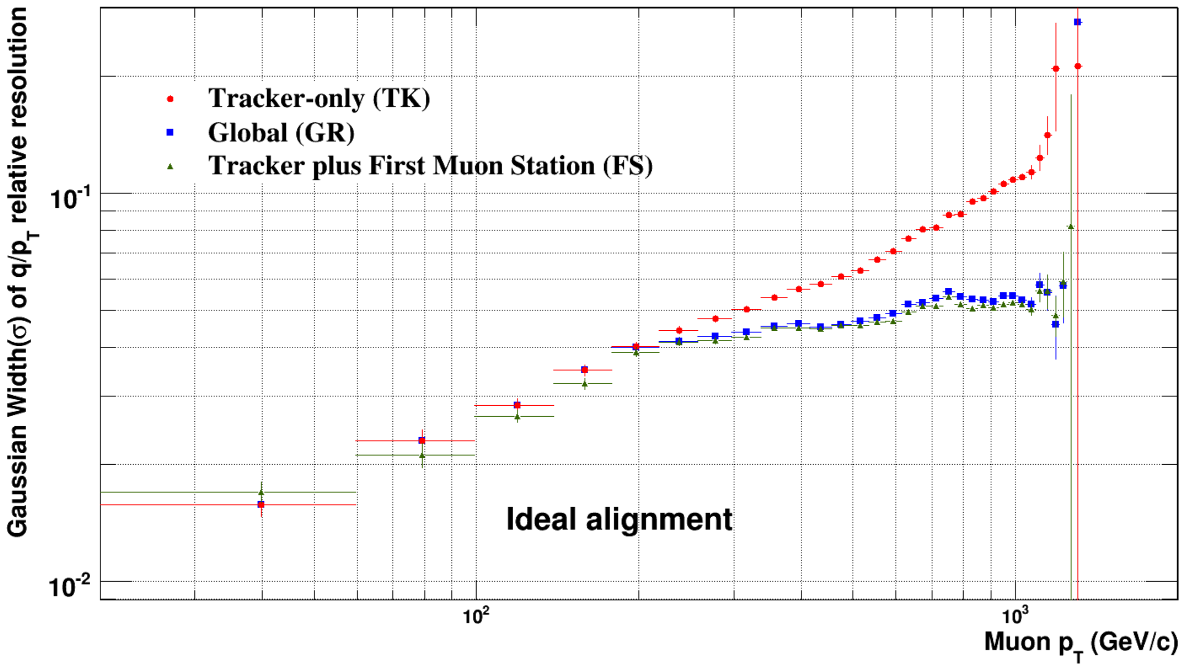

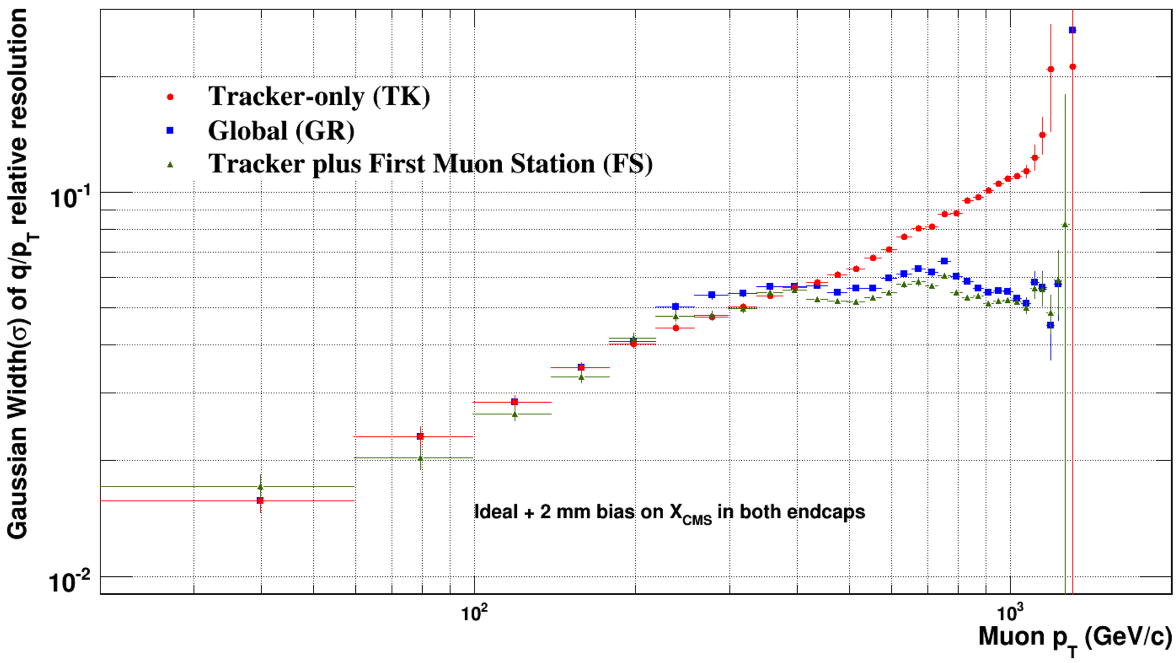

Figure 8: Relative muon p_T resolution vs. p_T for barrel and endcap muons based on Gaussian widths of $(q/p_T(\text{rec.}) - q/p_T(\text{gen.}))/q/p_T(\text{gen.})$ distributions for each p_T bin using the MC sample for $M_{Z'} = 2$ TeV$/c^2$ and three muon reconstructions for ideal alignment scenario (top) and with 2 mm systematic bias in x_{CMS} to all Muon Endcap stations (bottom)

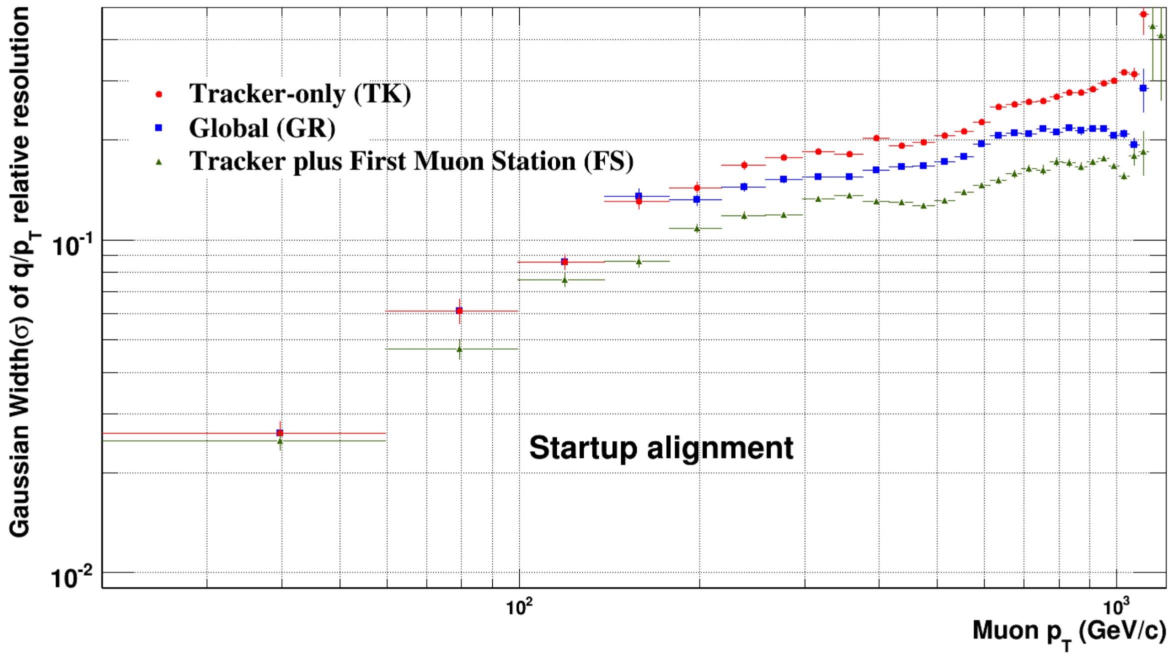

Figure 9: Relative muon p_T resolution vs. p_T for barrel and endcap muons based on Gaussian widths of $(q/p_T(\text{rec.}) - q/p_T(\text{gen.}))/q/p_T(\text{gen.})$ distributions for each p_T bin using the MC sample for $M_{Z'} = 2$ TeV$/c^2$, startup alignment scenario, and three muon reconstructions.

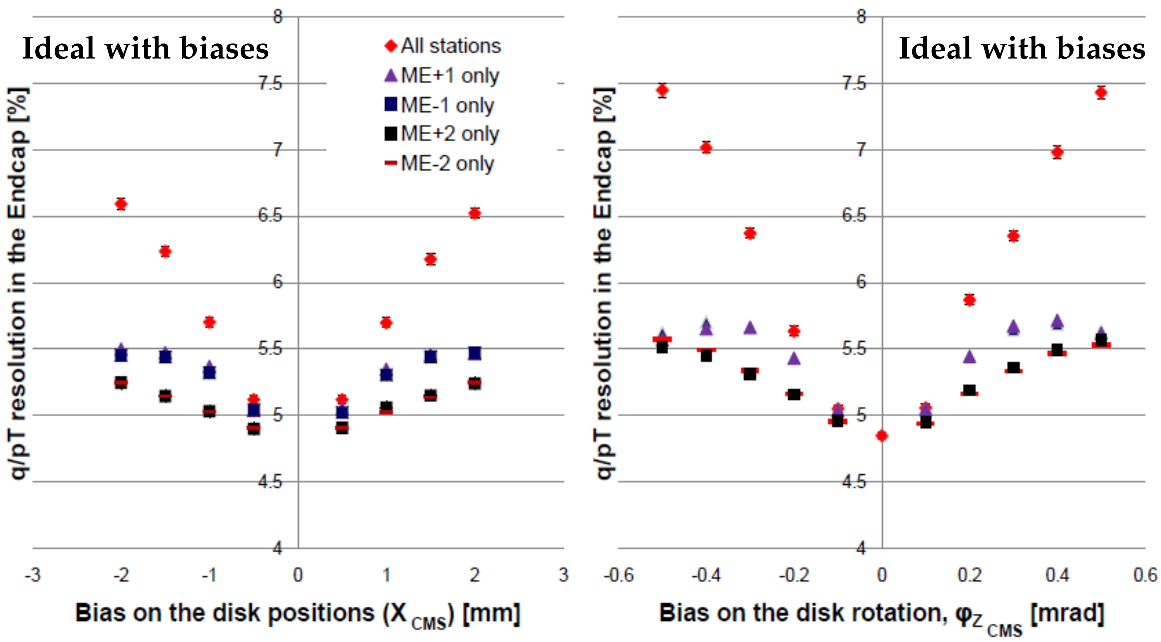

Figure 10: Relative muon p_T resolution vs. biases in the ideal endcap disk alignment for endcap muons based on Gaussian widths of $(q/p_T(\text{rec.}) - q/p_T(\text{gen.}))/q/p_T(\text{gen.})$ distributions using the MC sample for $M_{Z'} = 2$ TeV$/\text{c}^2$. Plots are for bias on muon endcap disk positions x_{CMS} (left) and bias on the disk rotation $\phi_{z_{CMS}}$ (right) applied to all Muon Endcap stations or individual stations ME+1, ME-1, ME+2, and ME-2.

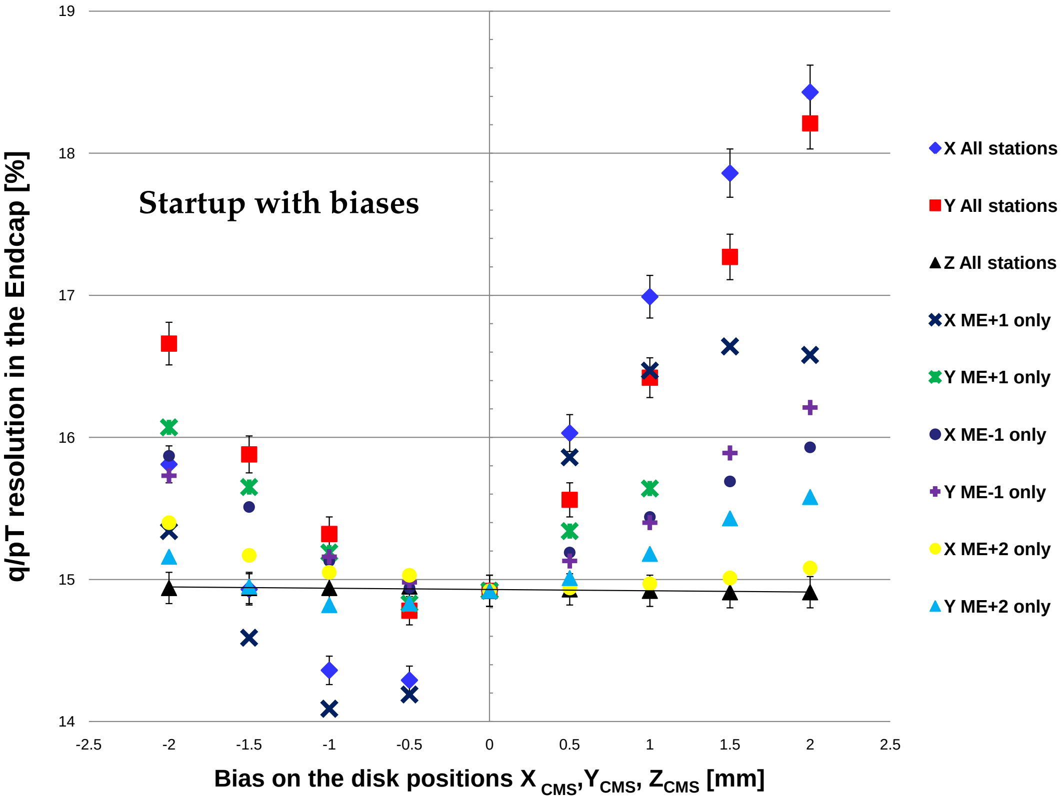

Figure 11: Relative muon p_T resolution vs. biases in startup endcap disk alignment for endcap muons based on Gaussian widths of $(q/p_T(\text{rec.})\text{-}q/p_T(\text{gen.}))/q/p_T(\text{gen.})$ distributions using the MC sample for $M_{Z'} = 2$ TeV/c^2. This plot shows the effect of biases on muon endcap disk positions x_{CMS}, y_{CMS}, and z_{CMS} applied to all Muon Endcap stations or individual stations ME+1, ME-1, ME+2, and ME-2.

6 CMS discovery potential in $Z' \rightarrow \mu^+\mu^-$ channel

6.1 Dimuon mass spectra and fitting procedure

An example of the dimuon mass $M_{\mu^+\mu^-}$ spectra for the full interference $Z'/Z^0/\gamma^*$ signal sample ($M_{Z'}$ = 1.2 TeV/c^2) and Drell-Yan background only samples are shown in figure 12; both reconstructed with the startup alignment. For the significance analysis, we use a background sample that is the weighted sum of these two background data sets. The resulting plot of signal and the weighted background is not shown here.

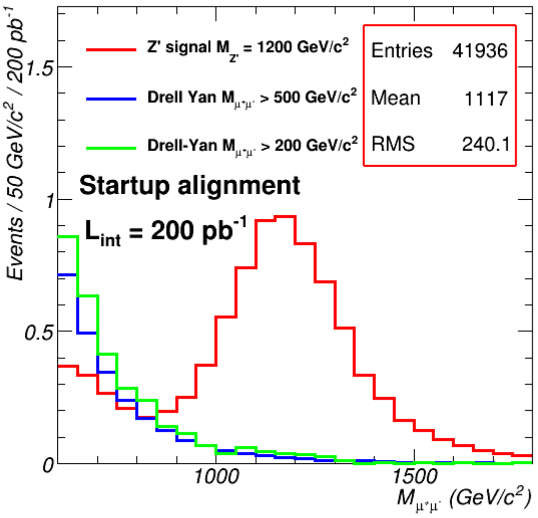

Figure 12: Histograms of the globally reconstructed dimuon invariant mass ($M_{\mu^+\mu^-}$) for the full interference $Z'/Z^0/\gamma^*$ signal sample ($M_{Z'} = 1.2\ TeV/c^2$) and Drell-Yan background Monte Carlo samples ($M_{\mu^+\mu^-} > 200 GeV/c^2$ and 500 GeV/c^2). The number of events per bin is normalized to an integrated luminosity of 200 pb^{-1}.

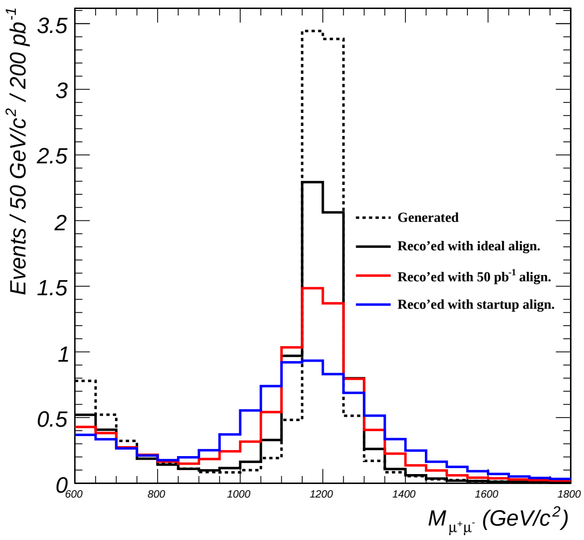

Figure 13: Histograms of the dimuon invariant mass ($M_{\mu^+\mu^-}$) for the full interference $Z'/Z^0/\gamma^*$ signal sample ($M_{Z'} = 1.2\ TeV/c^2$) at the event-generator level (dotted black line) and fully reconstructed with different alignments (solid lines with different colors). The number of events per bin is normalized to an integrated luminosity of 200 pb^{-1}.

Another example of dimuon mass spectra for the full interference $Z'/Z^0/\gamma^*$ signal for mass $M_{Z'}$ = 1.2 TeV/c^2, with or without detector and reconstruction related effects, is shown in Figure 13. The dotted black line in the plot shows the generated mass spectrum (100 % efficiency with no detector and reconstruction related effects). It is compared with fully reconstructed events for different alignment scenarios, i.e. ideal, 50 pb^{-1}, and startup alignments. Figure 13 clearly shows the effect of alignment on the mass resolution and how the peaks get widened with worsening alignment.

We focus on the regime close to the discovery limit, which is characterized by a modest number of accumulated events. We use ensembles of Monte Carlo pseudo-experiments selected from the large-statistics signal and background samples. The number of events in each experiment, N$_{evt}$, fluctuates according to a Poisson distribution with a mean of $\sigma\times$ Br $\times \int Ldt \times \epsilon$, where $\int Ldt$ is the integrated luminosity and ϵ is the combined trigger and reconstruction efficiency. The mass distribution is composed of $M_{\mu^+\mu^-}$ values for N$_{evt}$ events satisfying all selection criteria and not yet used in previous MC pseudo-experiments.

An unbinned maximum likelihood fit of the $M_{\mu^+\mu^-}$ values in each MC experiment is appropriate to test for the existence of a resonance and to measure its parameters if it is found to exist. We follow the methods discussed in section 5 of [20] for the fitting of dimuon mass spectra. As a model of the probability density function (pdf), p, of the parent population of the observed mass spectra, we use

$$p\left(M_{\mu^+\mu^-}; f_s, m_0, \Gamma, \sigma\right) = f_s \cdot p_s(M_{\mu^+\mu^-}; m_0, \Gamma, \sigma) + (1 - f_s) \cdot p_b(M_{\mu^+\mu^-}) \tag{3}$$

where

- p_s, the pdf of the signal, is a convolution of a Breit-Wigner signal resonance shape with a Gaussian accounting for mass resolution smearing.
- p_b, the pdf of the background, is modeled as an exponential, $e^{-k \cdot M_{\mu^+\mu^-}}$, with the parameter k determined from fits to Drell-Yan events. This pdf, using k = 2.0, gives a good description of the background shape in the whole mass region between 400 and 5000 GeV/c^2 [10].

There are three free parameters in the fit: the signal fraction $f_s = N_s/(N_s + N_b)$, the mass peak m_0, and the full width at half maximum (FWHM), Γ, of the signal. The shape of the background distribution is fixed, while its level is determined by the fit: f_s is a free parameter. Therefore, the fit explores the difference in shape between the signal and the background.

6.2 Z' signal significance analysis

We use a signal significance estimator $S_{\mathcal{L}}$ based on log-likelihood ratio, which was found to perform well in the search for Z' bosons from the previous study described in [25]:

$$S_{\mathcal{L}} = \sqrt{2\, ln\, (\mathcal{L}_{s+b}/\mathcal{L}_b)}\,, \tag{4}$$

where $\mathcal{L}_{s+b}$ is the maximum likelihood value obtained in the full signal-plus-background unbinned maximuom likelihood fit, and $\mathcal{L}_b$ is the maximum likelihood from the unbinned background only fit.

We use the method described in section 6.1 and the likelihood ratio estimator $S_{\mathcal{L}}$ to evaluate the CMS discovery potential for $Z' \to \mu^+\mu^-$. We calculate the statistical significance of various expected signal and background samples by using Monte Carlo calculation and fits described in section 6.1. We present estimated results for the mass range in which CMS can discover Z' bosons with a given amount of data for different detector alignment scenarios or correspondingly the required integrated luminosity to discover a Z' of a certain mass for different detector alignment scenarios.

All available Z' samples with different masses and misalignment scenarios are considered; the evaluation is repeated for several integrated luminosities. Two examples of signal significance distributions with the Gaussian fit, obtained from fits to a 1.2 TeV/c^2 Z'_{SSM} for an integrated luminosity of 200 pb^{-1} with startup alignment and with 50 pb^{-1} alignment, are shown in figure 14. A summary of the signal significance expected for the Z'_{SSM} at two signal mass points for an integrated luminosity of 200 pb^{-1} with startup, 50 pb^{-1}, and ideal alignment scenarios are tabulated in Table 6. We observe that better alignment improves the signal significance.

We use the same combinations of luminosities and misalignment scenarios to calculate the integrated luminosity needed to reach 5σ significance ($S_{\mathcal{L}} = 5$) for a Z'_{SSM} discovery. In Figure 15, we plot the signal significance as a function of integrated luminosity for two signal mass

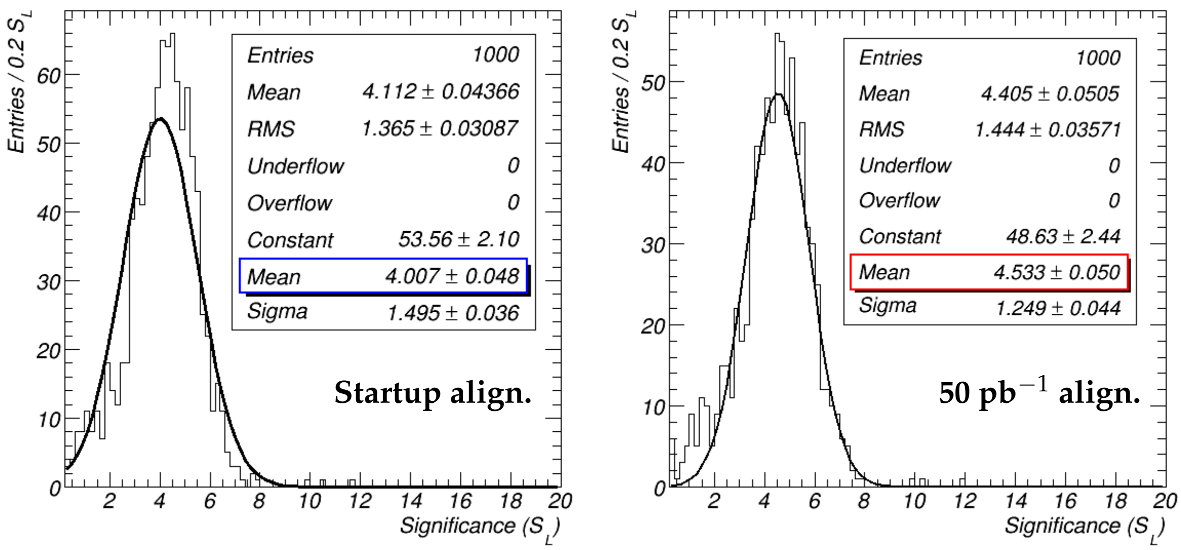

Figure 14: Histograms of signal significance for 1000 pseudo-experiments with the Gaussian fit for a 1.2 TeV/c^2 Z'_{SSM} for an integrated luminosity of 200 pb^{-1} with startup (left) and 50 pb^{-1} (right) alignments.

Table 6: Average values of the log-likelihood ratio significance estimator $S_{\mathcal{L}}$ for the Z'_{SSM} at two signal mass points for an integrated luminosity of 200 pb^{-1} with three alignment scenarios.

	Z'_{SSM} mass	
Alignment Scenario	1.0 TeV/c^2	1.2 TeV/c^2
Startup	6.7	4.0
50 pb^{-1}	7.8	4.5
Ideal	8.1	4.6

points for startup alignment and 50 pb^{-1} alignment. We connect the data points by a spline curve and extract the integrated luminosity required for 5σ for a given alignment. For example, on the average 250 pb^{-1} data are required to discover a Z' with mass M = 1.2 TeV/c^2 assuming the 50 pb^{-1} alignment from the Figure 15 (right). The integrated luminosity needed to reach 5σ significance as a function of Z'_{SSM} mass for three different alignment scenarios is shown in Figure 16, which is our summary plot for the discovery potential and the effect of alignment on the Z' search.

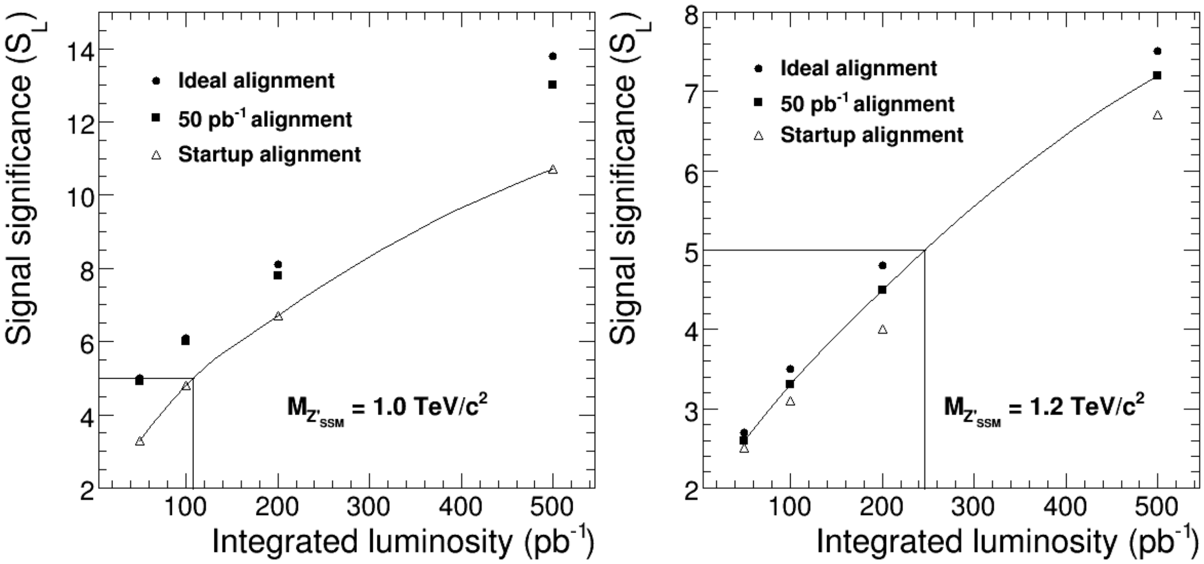

Figure 15: Signal significance as a function of the integrated luminosity and the alignment scenarios; the integrated luminosity needed to reach on the average 5σ significance ($S_{\mathcal{L}} = 5$) for the Z'_{SSM} is indicated.

From Figure 16, we conclude that

- A better aligned detector requires less data to reach the same signal significance.
- 80 pb^{-1} of data, and the tracker and the muon detectors aligned with 50 pb^{-1} should be sufficient to discover a Z'_{SSM} at 1 TeV/c^2.
- At least 250 pb^{-1} data are required to observe Z'_{SSM} boson with mass M = 1.2 TeV/c^2.

Muon endcap misalignments and the Z'_{SSM} signal significance

We have also used the samples with systematic muon endcap misalignment biases and calculated the average Z'_{SSM} (M=1.2 TeV/c^2) signal significance. The signal significance is plotted in figure 17 against the biases in position (left) and rotation around the beam line (right) of the entire endcap disks. It can be seen that the significance is sensitive to the misalignment of muon endcaps, but the effect is very small for our studied range of the misalignments, i.e. up to 2 mm in translation and up to 0.5 mrad in rotation around the beam line.

7 Summary and conclusions

Monte Carlo signal samples for $Z'_{SSM} \to \mu^+\mu^-$ in pp collisions at 7 TeV center-of-mass energy are generated and reconstructed for different Z' masses (1 TeV/c^2, 1.2 TeV/c^2, 1.3 TeV/c^2, and 2 TeV/c^2) with three different alignment scenarios. Two Monte Carlo samples for the dominant and irreducible Drell-Yan background are also generated for $M_{\mu^+\mu^-} > 200$ GeV/c^2 and

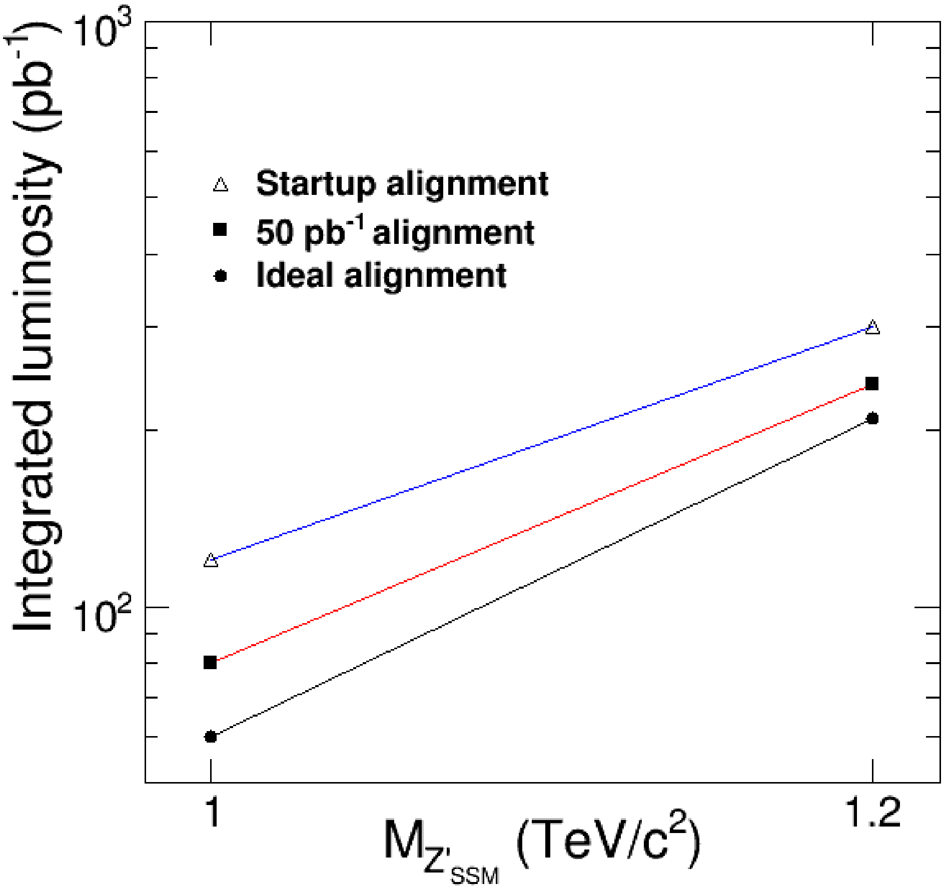

Figure 16: Integrated luminosity needed to reach 5σ significance ($S_{\mathcal{L}} = 5$) as a function of the mass of the Z'_{SSM} resonance reconstructed with ideal, startup, and 50 pb^{-1} alignments.

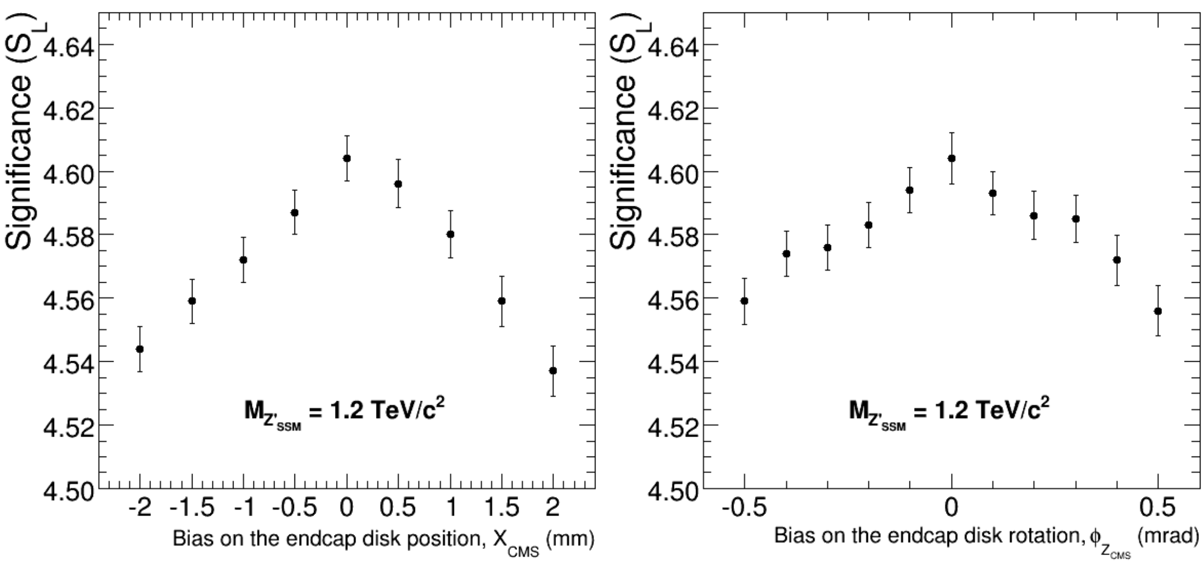

Figure 17: Average Z'_{SSM} signal significance as a function of the bias on the x_{CMS} position (left) and rotation around the beam line (right) of the muon endcap disks for $M_{Z'_{SSM}}$ = 1.2 TeV$/c^2$ using ideal alignment.

$M_{\mu^+\mu^-} > 500$ GeV/c^2. The 50 pb^{-1} alignment scenario is validated with this study. The muon transverse momentum and the dimuon mass resolutions are calculated with three muon reconstructions for the combinations of alignment scenarios, center-of-mass energies for different Z' masses. We find the global muon momentum resolution in the endcap 14.4% (4.8%) with the startup (ideal) alignment using the 1.2 TeV/c^2 Z'_{SSM} sample. The dimuon mass resolution is found to be 10.3% (3.2%) for the startup (ideal) alignment using the 1.2 TeV/c^2 Z'_{SSM} sample. An alignment systematics study is presented by varying the position or orientation of endcap stations with respect to ideal or startup alignment scenarios. We find a symmetrical effect on resolution with positive bias or negative bias and similar results for biases in x_{CMS} or y_{CMS}, when using the ideal alignment scenario, but not with the startup alignment scenario, which produces asymmetrical results. With the bias in z_{CMS} applied to all stations together, the resolution stays the same as without bias. With a misalignment of 2 mm in x_{CMS} or y_{CMS} position on ideal alignment scenario of all stations, the p_T resolution in the endcap worsens by about 2%.

We evaluate the discovery potential for $Z' \rightarrow \mu^+\mu^-$ in pp collisions at 7 TeV center-of-mass energy for different muon misalignments. We calculate the Z'_{SSM} signal significance as a function of integrated luminosity and estimate the required data for 5σ for two signal mass points. About 80 pb^{-1} of data and at least 250 pb^{-1} data with an aligned detector are required to discover a Z'_{SSM} with mass M = 1 TeV/c^2 and 1.2 TeV/c^2, respectively. We study the effect of muon endcap only misalignments on the Z' search and find a very small effect on the Z'_{SSM} signal significance.

Acknowledgments

We are grateful to all members of the CMS muon alignment group, Exotica muon and resonance groups, and in particular the UCLA group, who developed the software packages used in this study. In particular, we would like to thank Jim Pivarski, Jordan Tucker, Piotr Traczyk, Martijn Mulders, and Meenakshi Narain for their technical assistance, scientific consultation and advice.

References

[1] P. Langacker, "The Physics of Heavy Z' Gauge Bosons", *Rev. Mod. Phys.* **81** (2008) 1199–1228, arXiv:0801.1345. doi:10.1103/RevModPhys.81.1199.

[2] Global Tags for Conditions Data, https://twiki.cern.ch/twiki/bin/viewauth/CMS/SWGuideFrontierConditions.

[3] Available Alignment Constants, https://twiki.cern.ch/twiki/bin/view/CMS/SWGuideAlignmentConstants.

[4] Scenarios for Mis-Alignment and Mis-Calibration for Monte Carlo Production, https://twiki.cern.ch/twiki/bin/view/CMS/AlCaScenarios.

[5] CMS Collaboration, "Alignment of the CMS muon system with cosmic-ray and beam-halo muons", *J. Instrum.* **5** (Nov, 2009) T03020. doi:10.1088/1748-0221/5/03/T03020.

[6] 50 pb^{-1} muon misalignment scenario (MC), https://hypernews.cern.ch/HyperNews/CMS/get/muon-alignment/342.html.

[7] Tracker Misalignment Scenarios, https://twiki.cern.ch/twiki/bin/view/CMS/TkMisalignmentScenariosCSA07.

[8] Zprime2muAnalysis package, http://cmssw.cvs.cern.ch/cgi-bin/cmssw.cgi/CMSSW/SUSYBSMAnalysis/Zprime2muAnalysis/.

[9] CMS Collaboration, "CMS Technical Design Report, Volume II: Physics Performance", *J. Phys.* **G34** (2007) 995–1579.

[10] R. Cousins, J. Mumford, and V. Valuev, "Detection of Z' Gauge Bosons in the Dimuon Decay Mode in CMS", *CMS Note* **2006/062** (2006).

[11] I. Belotelov et al., "Search for Randall-Sandrum Graviton Decay into Muon Pairs", *CMS Note* **2006/104** (2006).

[12] V. Valuev, "Evaluation of CMS Discovery Potential in the $Z' \to \mu^+\mu^-$ Channel at $\sqrt{s} = 6$ and 10 TeV", *CMS AN Note* **2009/017** (2009).

[13] T. Sjostrand, S. Mrenna, and P. Skands, "PYTHIA 6.4 physics and manual", *JHEP* **05** (2006) 026, arXiv:hep-ph/0603175v2.

[14] J. Pumplin et al., "New generation of parton distributions with uncertainties from global QCD analysis", *JHEP* **07** (2002) 012, arXiv:hep-ph/0201195.

[15] M. R. Whalley, D. Bourilkov, and R. C. Group, "The Les Houches Accord PDFs (LHAPDF) and Lhaglue", arXiv:hep-ph/0508110.

[16] P. Langacker, R. W. Robinett, and J. L. Rosner, "New heavy gauge bosons in pp and $p\bar{p}$ collisions", *Phys. Rev. D* **30** (Oct, 1984) 1470–1487. doi:10.1103/PhysRevD.30.1470.

[17] P. Langacker, "Z' Physics at the LHC", arXiv:0911.4294.

[18] CMSSW Reference Manual, https://cms-cpt-software.web.cern.ch/cms-cpt-software/General/gendoxy-doc.php.

[19] CMS Collaboration, “The CMS Physics Technical Design Report, Volume I”, *CERN/LHCC* **2006-001** (2006).

[20] M. Chen et al., “Search for New High-Mass Resonances Decaying to Muon Pairs in the CMS Experiment”, *CMS AN* **2007/038** (2007).

[21] CMS Collaboration, “Aligning the CMS Muon Chambers with the Muon Alignment System during an Extended Cosmic Ray Run”, *J. Instrum.* **5** (Nov, 2009) T03019. 35 p. `doi:10.1088/1748-0221/5/03/T03019`.

[22] CMS Collaboration, “Performance of CMS Muon Reconstruction in Cosmic-Ray Events”, *J. Instrum.* **5** (Nov, 2009) T03022. `doi:10.1088/1748-0221/5/03/T03022`.

[23] J. Pivarski et al., “Confirmation of the Effect of RPC Hits and Updated Alignment without RPC Bias”, *CMS Muon Alignment Meeting*. (28 May, 2010).

[24] Software Guide for Muon Geometry Conversion, https://twiki.cern.ch/twiki/bin/viewauth/CMS/SWGuideMuonGeometryConversion.

[25] R. Cousins, J. Mumford, and V. Valuev, “Detection of Z' Gauge Bosons in the Dimuon Decay Mode in CMS”, *CMS Note* **2005/002** (2005).